EuroSun2026

Effects of Collector Type and Control Strategy on the Performance of PV/T Heat Pump Systems

Matthias Teupel[1], Thomas Blum[1]

[1] *Rud. Otto Meyer Technik GmbH and Co. KG (ROM Technik) Research and Development, Hamburg (Germany)*

mteupel@rom-technik.de

thblum@rom-technik.de

Summary

This simulation study investigates the combined influence of the wind and infrared sensitive collector (WISC) type and the control strategy on the performance of a photovoltaic-thermal (PV/T) brine-to-water heat pump system for an industrial application. A Modelica-based PV/T model is developed using ISO 9806:2025 and Solar Keymark parameters to represent finned and non-finned WISCs. Three source-side control strategies (On-Off, Solar, Continuous) are evaluated together with homogeneous and mixed collector field configurations. Annual simulations show a 9 % higher seasonal performance factor (SPF_{Grid}) for finned collectors than for the non-finned WISC, while a mixed field achieves similar performance to the finned type at 10 % lower investment cost. Among the three control strategies, the Continuous yields the highest SPF_{Grid} for both WISC types. A detailed analysis shows that the influence of the control strategy on system performance is stronger for the non-finned than for the finned WISC type.

Keywords: PV/T, WISC type, heat pump, source-side control strategies, mixed collector fields, Modelica

Field of application for the findings: Industrial PV/T heat pump systems, mixed collector field design

Addressed audience: Researchers and engineers in PV/T heat pump and solar energy systems

1. Introduction

The combination of unglazed PV/T collectors, utilized for ambient and solar heat gains, with a brine-to-water heat pump facilitates an energy-efficient and low-carbon heat supply (Del Amo et al., 2019). While such systems are particularly attractive for densely built urban areas due to their noise-free operation (Kramer, 2024), their application in the residential sector is limited by available roof area (Epp, 2025). Industrial applications with large roof areas therefore represent a viable alternative. Since previous research has focused predominantly on residential buildings (Kramer et al., 2025), this study addresses an industrial application, characterized by thermal loads independent of ambient temperature, in addition to space heating.

Solar Keymark investigations of WISCs with and without fins show opposing thermal behavior based on standardized testing and certified measurements (International Organization for Standardization, 2025; Solar Keymark, 2024, 2025). While finned WISCs can be characterized as air-brine collectors, with primarily ambient thermal gains, non-finned alternatives perform better under solar irradiation. Experimental studies have primarily focused on systems employing a single collector type (Del Amo et al., 2019; Leibfried et al., 2020; Ramos et al., 2019; Fudholi and Sopian, 2018), while Chhugani et al. (2023) compared both types in a simulation study for the monovalent heat supply of a single-family house. A direct comparison of finned and non-finned WISC types in an industrial application has not yet been reported. The opposing thermal performance characteristics of finned and non-finned WISCs may be combined through a shared hydraulic configuration, potentially enabling synergistic effects within a PV/T heat pump system. However, the performance of such a mixed configuration incorporating different WISC types has not yet been investigated.

Unlike air-source heat pumps, PV/T heat pump systems can store thermal energy on the source side. Source-side control strategies for PV/T heat pump systems have been investigated in simulation studies (John and Kaltschmitt, 2022; Hengel et al., 2020; Ma et al., 2021) as well as in experimental field tests (Del Amo et al., 2019; Mbuwir et al., 2024; Jiang et al., 2025). Although these approaches achieve efficient system operation, further development is required to maximize the PV self-consumption rate. The influence of the WISC type on the effectiveness of such control strategies has not yet been investigated in detail.

So far, the effects of WISC type and source-side control strategy on PV/T heat pump systems have been investigated separately. Consequently, this paper presents a numerical simulation study investigating the influence of the WISC type on the efficiency of source-side control strategies, as well as the effects of the WISC type and source-side control strategy on overall system performance in an industrial application. To this end, a PV/T model is developed in Modelica, an equation-based simulation language (Modelica Association, 2026). Furthermore, the control strategies proposed by Ma et al. (2021) and Hengel et al. (2020) are extended and evaluated. Moreover, this study presents the first techno-economic analysis of PV/T systems with mixed collector fields.

2. PV/T Test Bench

A test bench was designed for the R&D laboratory of ROM Technik in Hamburg (Germany) to conduct the planned investigations. Two identically sized collector fields, brine storage tanks, and brine-to-water heat pumps enable a direct comparison of WISC types and control strategies with respect to system efficiency. On the sink side, both heat pumps supply a 5 m^3 buffer storage tank for space heating. A schematic overview of the system is shown in Figure 1.

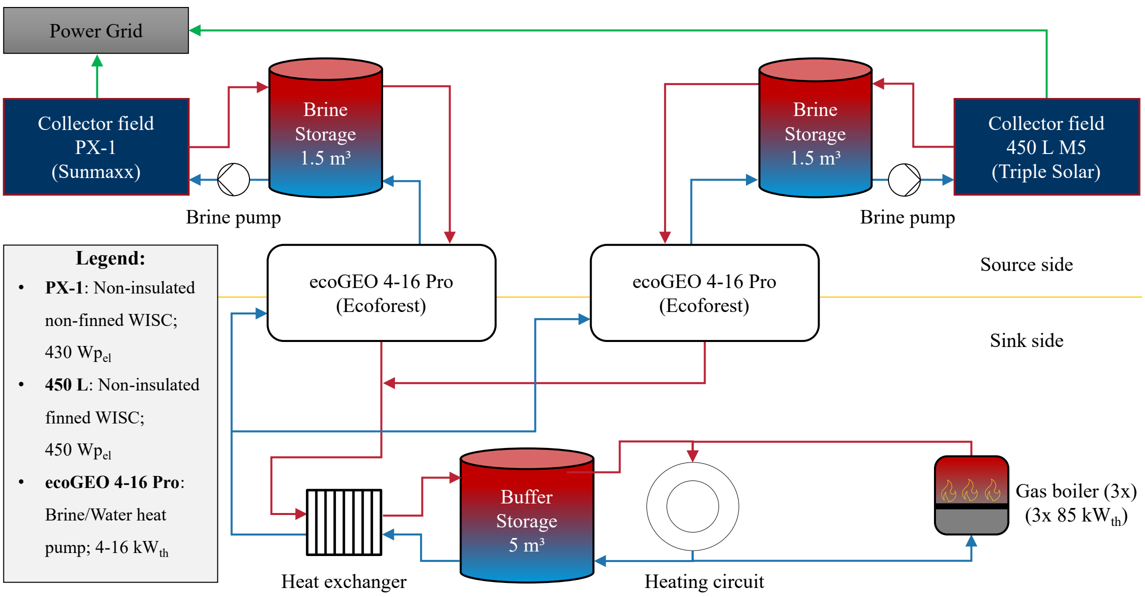

Fig. 1: Schematic of the PV/T heat pump test bench. Collector fields are not in mixed configuration.

Since the test bench is still under construction, a simulative representation is developed for this study. As the planned test bench represents a complex system with multiple interacting subsystems and dynamic operating conditions, the equation-based modeling language Modelica is used for its implementation (Modelica Association, 2026). The subcomponents and the underlying model are described in the following.

2.1 Heat Pump

Two R-290-based brine-to-water heat pumps (ecoGEO+ B 4-16 PRO, Ecoforest) with a modulation range of 4 to 16 kW_{th} are used. The simulation is implemented using the HKESim Modelica library, which has been further developed by the ROM Technik R&D department. HKESim is based on the HKSim library developed by Wischhusen (2005). The library includes a heat pump model that calculates the condenser heat output $\dot{Q}_{con}$

and electrical power consumption $P_{\mathrm{el,hp}}$ based on characteristic curves for heating capacity and coefficient of performance (COP) as functions of the brine and water temperature. Part-load operation is represented by a partial-load factor derived from manufacturer data, which accounts for the influence of compressor speed on heat pump performance. The manufacturer's data provide a realistic representation of part-load and full-load operation across a wide range of brine and water temperatures. The required condenser heat output $\dot{Q}_{\mathrm{req,hp}}$ is determined from the water-side mass flow rate $\dot{m}_{\mathrm{con}}$, the specific heat capacity c_p, and the temperature difference between the condenser inlet temperature $T_{\mathrm{con,in}}$ and the setpoint temperature $T_{\mathrm{set,hp}}$:

$$\dot{Q}_{\mathrm{req,hp}} = \dot{m}_{\mathrm{con}}\, c_p \left(T_{\mathrm{set,hp}} - T_{\mathrm{con,in}}\right) \tag{1}$$

The actual thermal output is then limited by the minimum and maximum heating capacities $\dot{Q}_{\mathrm{min}}$ and $\dot{Q}_{\mathrm{nom,hp}}$ (operating limits) derived from the characteristic curves:

$$\dot{Q}_{\mathrm{con}} = \dot{Q}_{\mathrm{th,hp}} = x_{\mathrm{hp}} \cdot \min\left(\max\left(\dot{Q}_{\mathrm{req,hp}}, \dot{Q}_{\mathrm{min}}\right), \dot{Q}_{\mathrm{nom,hp}}\right), \qquad x_{\mathrm{hp}} \in \{0, 1\} \tag{2}$$

The heat pump operation is governed by a binary enable signal x_{hp}. For $x_{\mathrm{hp}} = 1$, the heat pump is enabled, whereas for $x_{\mathrm{hp}} = 0$, the heat pump is disabled and the thermal output is set to zero.

The electrical power consumption $P_{\mathrm{el,hp}}$ is calculated from the resulting COP:

$$P_{\mathrm{el,hp}} = \frac{\dot{Q}_{\mathrm{th,hp}}}{\mathrm{COP}} \tag{3}$$

2.2 Thermal Storage Units

The two 1.5 m^3 brine storage units and the 5 m^3 buffer storage tank on the sink side of the heat pumps are modeled using the detailed storage models of the AixLib library (Maier et al., 2026). These models provide a detailed representation of the thermal storage tanks, including thermal stratification and heat losses. The storage volume is discretized into multiple layers, allowing the temperature distribution within the tank to be spatially resolved. Heat transfer between adjacent layers and buoyancy-driven mixing effects are all considered in the model.

2.3 PV/T Collector

A two-node PV/T Modelica model is developed to represent the opposing thermal behavior of the two WISC types. The model is integrated into HKESim and extends the existing PV model. The electrical model calculates the cell temperature and the resulting electrical power output based on solar irradiance, ambient temperature, wind speed, and collector orientation. Solar radiation incident on the tilted collector surface, G_{tilt}, is determined using a transposition model that accounts for beam irradiance G_{beam}, diffuse irradiance G_{diff}, ground-reflected irradiance G_{refl}, and optical losses due to the glazing. In this context, G_{beam}, G_{diff}, and G_{refl} denote the direct, diffuse, and ground-reflected irradiance components used in the irradiance transposition model, whereas G_{b} and G_{d} in Equation 5 denote the direct and diffuse solar irradiance incident on the collector according to the ISO 9806:2025 thermal collector performance model. The underlying methodology is based on established solar engineering approaches described by Quaschning (2023) and Duffie and Beckman (2013). The electrical power output is subsequently calculated from the resulting cell temperature and the current-voltage characteristics of the PV module.

The irradiance on the tilted collector surface is calculated as:

$$G_{\mathrm{tilt}} = G_{\mathrm{beam}} R_b + G_{\mathrm{diff}} + G_{\mathrm{refl}}, \tag{4}$$

Where R_b denotes the geometric conversion factor from horizontal to tilted irradiance.

The thermal model follows the calculation methodology of ISO 9806:2025 and is parameterized using Solar Keymark measurements (International Organization for Standardization, 2025). The thermal power calculation is based on a two-node model as proposed by Lämmle (2018), which represents the collector by a fluid node and a PV cell node linked through thermal coupling. Depending on the selected test method, the thermal performance is calculated using either the steady-state or the quasi-dynamic procedure as defined in ISO 9806:2025. In both approaches, thermal power is determined from solar irradiance, mean fluid temperature, ambient temperature, wind speed, and long-wave radiation. The model additionally accounts for wind-dependent heat losses and long-wave radiative exchange with the environment.

The quasi-dynamic thermal power output is calculated as:

$$\begin{aligned}\dot{Q}_{\mathrm{th,col}} = A_{\mathrm{G}}\Big[&\eta_{0,b}K_bG_b + \eta_{0,b}K_dG_d - a_1(\vartheta_m - \vartheta_a) - a_2(\vartheta_m - \vartheta_a)^2 - a_3u_{\mathrm{wind}}(\vartheta_m - \vartheta_a)\\ &+a_4\left(E_L - \sigma T_{\mathrm{a}}^4\right) - a_5\frac{\mathrm{d}\vartheta_m}{\mathrm{d}t} - a_6u_{\mathrm{wind}}(K_bG_b + K_dG_d) - a_8(\vartheta_m - \vartheta_a)^4\Big]\end{aligned} \tag{5}$$

For the steady-state approach, the transient term $a_5\frac{\mathrm{d}\vartheta_m}{\mathrm{d}t}$ is omitted and the direct and diffuse irradiance components are replaced by the hemispherical irradiance formulation specified in ISO 9806:2025. The constants and variables used in Equation 5 are defined in the nomenclature 7. For validation of the thermal model, the simulation results were compared with several Solar Keymark test points.

For a more accurate assessment of the additional electrical yield resulting from PV cell cooling under solar irradiance, an additional absorber surface temperature node and an explicit thermal coupling model between the absorber and the PV cells would be required. The present two-node approach is not suitable for a detailed comparison of the cooling-induced electrical benefits of the two WISC types. Therefore, the analysis primarily focuses on their thermal performance.

In the field of PV/T collectors, WISCs are used in monovalent brine-to-water heat pump systems by harvesting heat from both ambient air and solar irradiation (Del Amo et al., 2019). The test bench is designed to compare two WISC concepts. The finned configuration is represented by the Triple Solar 450-L collector, while the Sunmaxx PX-1 is used as the non-finned alternative. Their opposing performance characteristics are illustrated in Figure 2.

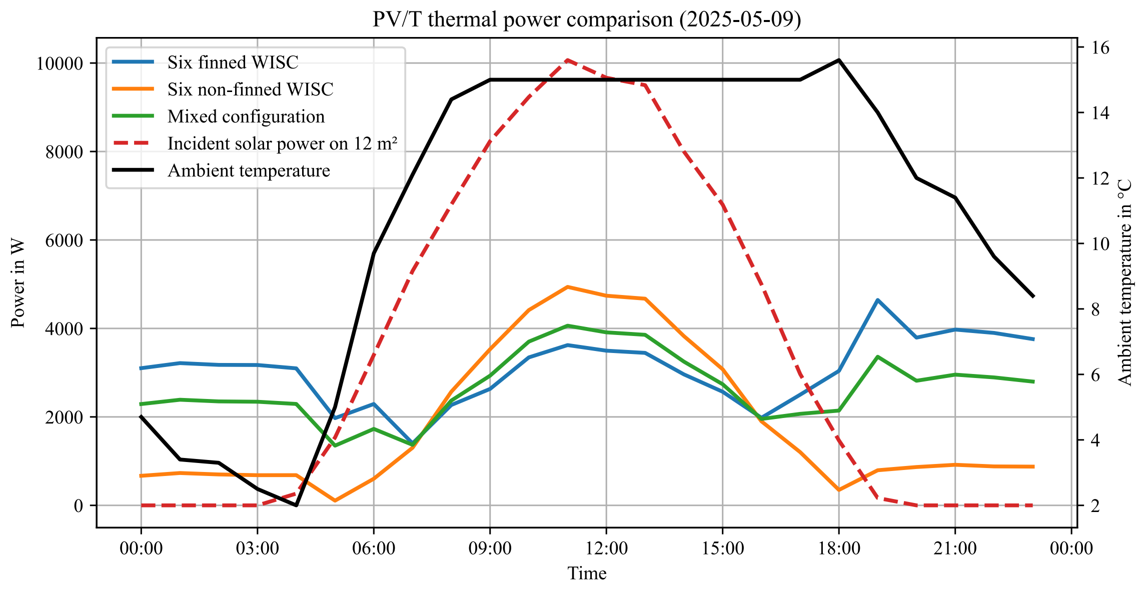

Fig. 2: Opposing thermal behaviour of finned and non-finned WISCs. Additionally, the thermal behavior of a mixed configuration of four finned and two non-finned WISCs is shown.

The figure shows a representative day in May for Hamburg and includes the thermal output of six finned and six non-finned collectors, together with the ambient temperature and the incident solar power on all six collectors. The thermal output of the WISCs was calculated using the PV/T model described above, while weather data were obtained from a nearby Deutscher Wetterdienst (DWD, German Meteorological Service) weather station. For simplicity, the temperature difference between the mean collector fluid temperature and the ambient temperature ($\vartheta_m - \vartheta_a$) was assumed to depend on solar irradiance, taking values of -1 K under high solar irradiation, -4 K under low solar irradiation, and -6 K in the absence of solar irradiation. Collector performance was calculated under steady-state conditions. It can be observed that the non-finned collector design provides a higher thermal output during periods of solar irradiation due to the direct thermal coupling between the fluid channels and the PV cells. In contrast, the fins of the finned design increase the heat exchange area exposed to the ambient air, and therefore enhance heat gains under low or no-irradiance conditions. A total of twenty-six finned and twenty-six non-finned WISCs are installed in the PV/T test bench to supply the heat pumps.

The combination of both WISC types in a mixed hydraulic configuration combines the ambient heat gains of the finned WISC with the solar heat gains of the non-finned alternative. A representative daily profile of such a mixed configuration is also shown in Figure 2. As illustrated in Figure 3, the individual WISCs are connected in parallel within each string, while the strings themselves are also connected in parallel. For the exemplary configuration, a ratio of two-thirds finned to one-third non-finned WISCs was selected.

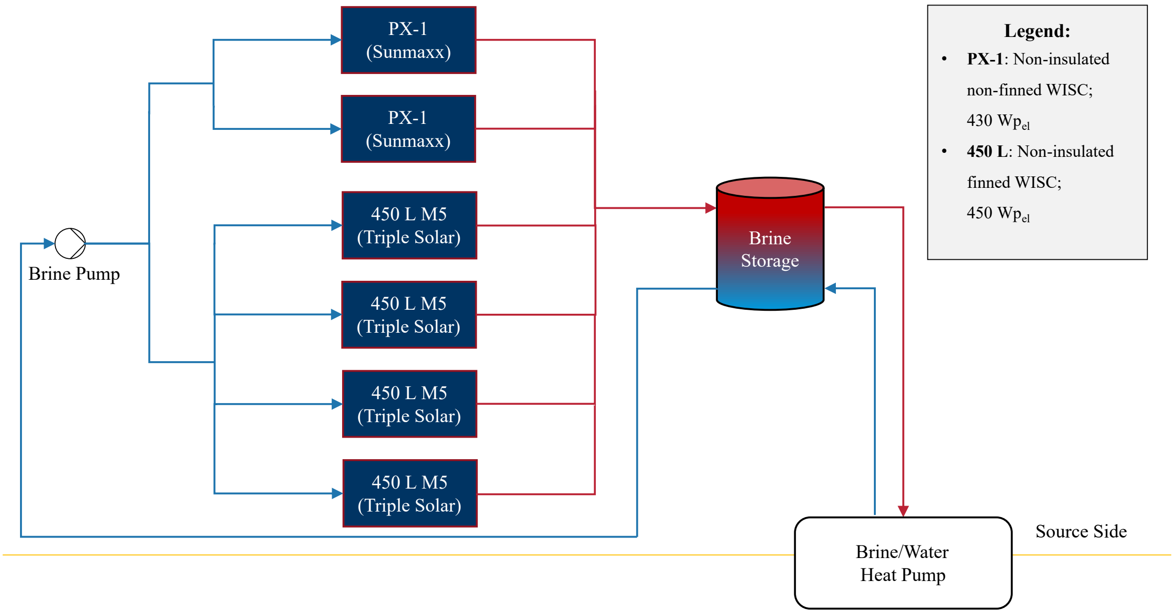

Fig. 3: Schematic of the mixed hydraulic source-side configuration for one heat pump in the PV/T heat pump test bench.

The remaining components, including the gas boilers, valves, mixing units, consumer, and sensors, are modeled using HKESim. A detailed description of the thermal load profile is provided in Section 5.

3. Control of the PV/T Heat Pump System

The control strategy is divided into source-side and sink-side control. As shown in Figure 1, the source-side circuit consists of the WISCs, the brine storage tanks, and the brine pump. The controlled variable is the bottom brine storage temperature, the manipulated variable is the speed of the brine pump, and the primary disturbances are the ambient temperature, the wind speed, and solar irradiance. For the source side of the heat pump, three control strategies are investigated:

- **On-Off control strategy**: This strategy is a further development of Method #1 introduced by Ma et al. (2021). A two-point controller regulates the temperature difference between the PV cell temperature and the bottom temperature of the brine storage. Pump activation and deactivation are defined by upper and lower dead bands of 5 °C and 2 °C, respectively. When the temperature difference exceeds the upper dead band, the brine pump is switched on; when it falls below the lower dead band, the pump is switched off. During operation, the brine pump runs at full speed.

- **Solar control strategy**: Building on the PV/T collector control strategy proposed by Hengel et al. (2020), the On-Off control strategy is extended by a four-step pump-speed control based on solar irradiance. In addition to the temperature-difference-based activation and deactivation logic, the pump speed is adjusted according to the available PV power. In the absence of PV power, the brine pump operates at base load, whereas sufficient PV surplus enables full-speed operation.
- **Continuous control strategy**: As an advancement of Method #2 proposed by Ma et al. (2021), a continuous feedback controller regulates the temperature difference between the PV cell temperature and the bottom temperature of the brine storage to a fixed setpoint of 2 °C. Similar to the Solar control strategy, the maximum pump speed is limited as a function of the available PV power.

As illustrated in Figure 1, the sink-side circuit consists of the heat pumps, the buffer storage tank, and the thermal consumer. The controlled variable is the buffer storage temperature, the manipulated variable is the heat pump operation, and the primary disturbance is the thermal load demand. The sink-side control strategy is determined by the buffer storage state of charge and implemented as a two-point controller that uses PV power surplus to charge the buffer above its nominal temperature setpoint. This approach reflects the current state of research and is described in detail by Wüllhorst et al. (2023).

4. Key Performance Indicator

The SPF_{Grid} is calculated to evaluate the overall efficiency of the PV/T heat pump system. It considers the supplied thermal energy and the electrical demand of both the heat pump and the brine pump, while subtracting the PV electricity used on-site. It should be noted that SPF_{Grid} is not a conventional system seasonal performance factor. Instead, it is defined here as a PV-adjusted grid-based performance indicator, relating the useful thermal energy delivered by the heat pump to the electricity imported from the grid for operation of the heat pump and brine pump:

$$SPF_{\text{Grid}} = \frac{Q_{\text{hp}}}{E_{\text{grid}}} = \frac{Q_{\text{hp}}}{E_{\text{grid,hp}} + E_{\text{grid,bp}}} \tag{6}$$

Where Q_{hp} is the thermal energy delivered by the heat pump, and $E_{\text{grid,hp}}$ and $E_{\text{grid,bp}}$ are the grid electricity imports attributed to the heat pump and brine pump, respectively. The grid electricity demand is determined on a time-step basis from the residual electrical load after allocation of the on-site consumed PV electricity:

$$P_{\text{grid}}(t) = \max\left[P_{\text{el,hp}}(t) + P_{\text{el,bp}}(t) - P_{\text{pv,allocated}}(t), 0\right] \tag{7}$$

The grid electricity imports E_{grid} are then obtained by integrating $P_{\text{grid}}(t)$ over the evaluation period. A higher SPF_{Grid} indicates a more efficient PV/T heat pump system. As the primary performance indicator of this study, it is used to evaluate and compare the influence of both the investigated control strategies and the different WISC types on the overall system performance.

5. Boundary Conditions and Simulation Variants

The investigated building complex of the R&D department of ROM Technik consists of an office building and two laboratory halls equipped with test benches for fluid dynamic and thermal engineering investigations. The buildings were constructed in 1973. In addition to the space heating demand, the load profile includes weather-independent peak loads resulting from laboratory operation. Consequently, the resulting heat demand profile is representative of a typical industrial application.

The heat pumps cover the base load, while the gas boilers provide peak load capacity. The PV/T collectors were installed with a tilt angle of 10° and an azimuth angle of 20° west of south. Each brine pump provides a maximum mass flow rate of $1.08\,\text{kg}\,\text{s}^{-1}$ ($3888\,\text{L}\,\text{h}^{-1}$), corresponding to a maximum mass flow rate of $0.04\,\text{kg}\,\text{s}^{-1}$ ($150\,\text{L}\,\text{h}^{-1}$) per collector for the field of 26 collectors (assuming ideal hydraulic balancing). The consumer model uses the measured load profile from 2025 of the building complex. Weather data corresponding to the load profile were obtained from a nearby DWD weather station in Hamburg Fuhlsbüttel. Simulations were performed with a 15 minute time step using the CVode solver and a solver tolerance of 0.0001.

The three control strategies were simulated for the planned investigations. The test bench design enables a direct comparison of the WISC types for each control strategy, allowing the influence of the collector type on the effectiveness of the control strategy to be assessed.

To evaluate the mixed hydraulic configuration, a parametric study was conducted in which the number of finned and non-finned WISCs was systematically varied while maintaining a constant total number of collectors. All possible combinations were investigated, ranging from one finned and twenty-five non-finned WISCs to twenty-five finned and one non-finned WISC.

All simulations were conducted over a one-year period. In addition, a four-day period in September was selected for detailed analysis to assess system behavior under industrial operating conditions with load profiles independent of ambient temperature.

6. Results

The results of the annual simulation are summarized in Table 1. On average across the three control strategies, the finned WISC type achieves a 9 % higher SPF_{Grid}, driven in part by a 4 % increase in heat pump thermal output. This advantage is mainly due to the finned heat exchanger, which enables higher thermal gains during periods of low or no solar irradiation compared to the non-finned WISC type.

For the four-day-period in September, Figure 4 presents the behavior of both WISCs and all three control strategies. For each case, the electrical power demand of the heat pump and the PV power output are shown. These data illustrate the operating periods of the heat pumps. For this period, whenever the PV power exceeds 4 $\mathrm{kW_{el}}$, the heat pump is operated at full load, while the buffer storage is charged beyond its nominal setpoint by means of the sink control strategy.

In addition, the thermal output of both WISCs is shown for the respective control strategies. During periods without solar irradiation, the finned WISCs provide higher thermal output than the non-finned WISCs for all three control strategies. In contrast, during periods with solar irradiation, the thermal outputs of both WISC configurations are at a comparable level. Furthermore, the temperature at the top of the brine storage is plotted. During periods with solar irradiation, the Continuous control strategy enables the highest storage-top temperatures for the non-finned WISCs. Although the thermal output remains at a similar level, as illustrated on 14 September at 12:00, the reduced volume flow rate results in a higher storage temperature. This effect can be observed for all three control strategies for the non-finned WISCs during periods with solar irradiation. Consequently, the heat pumps operate more efficiently under these conditions.

The thermal demand in the investigated application consists partly of load periods that are independent of ambient temperature; however, space-heating demand dominates over the course of the year. The highest thermal loads occur during periods of low or no solar irradiation. Consequently, the finned WISC type enables more efficient and higher-yield system operation for all three control strategies. When thermal load is present, the supply temperature predominantly exceeds 60 °C, which explains the magnitude of the observed SPF_{Grid} values.

Tab. 1: Results of annual simulation and investigation period in September (in brackets).

Control Strategy	$SPF_{\mathrm{Grid,finned}}$	$SPF_{\mathrm{Grid,non-finned}}$	$Q_{\mathrm{th,hp,finned}}$ in MWh	$Q_{\mathrm{th,hp,non-finned}}$ in MWh
On-Off	3.12 (4.57)	2.86 (4.31)	49.6 (0.475)	47.6 (0.473)
Solar	3.16 (4.70)	2.91 (4.51)	49.3 (0.487)	47.5 (0.486)
Continuous	3.17 (4.73)	2.92 (4.56)	49.3 (0.486)	47.5 (0.485)

A parameter study was carried out to determine the optimal distribution of the two WISC types for the mixed collector field configuration of this application. In all configurations, a total of twenty-six WISCs were installed to supply a single heat pump. As illustrated in Figure 3, all WISCs were connected in parallel. The analysis was conducted for the four-day period in September introduced above, as it is representative of industrial

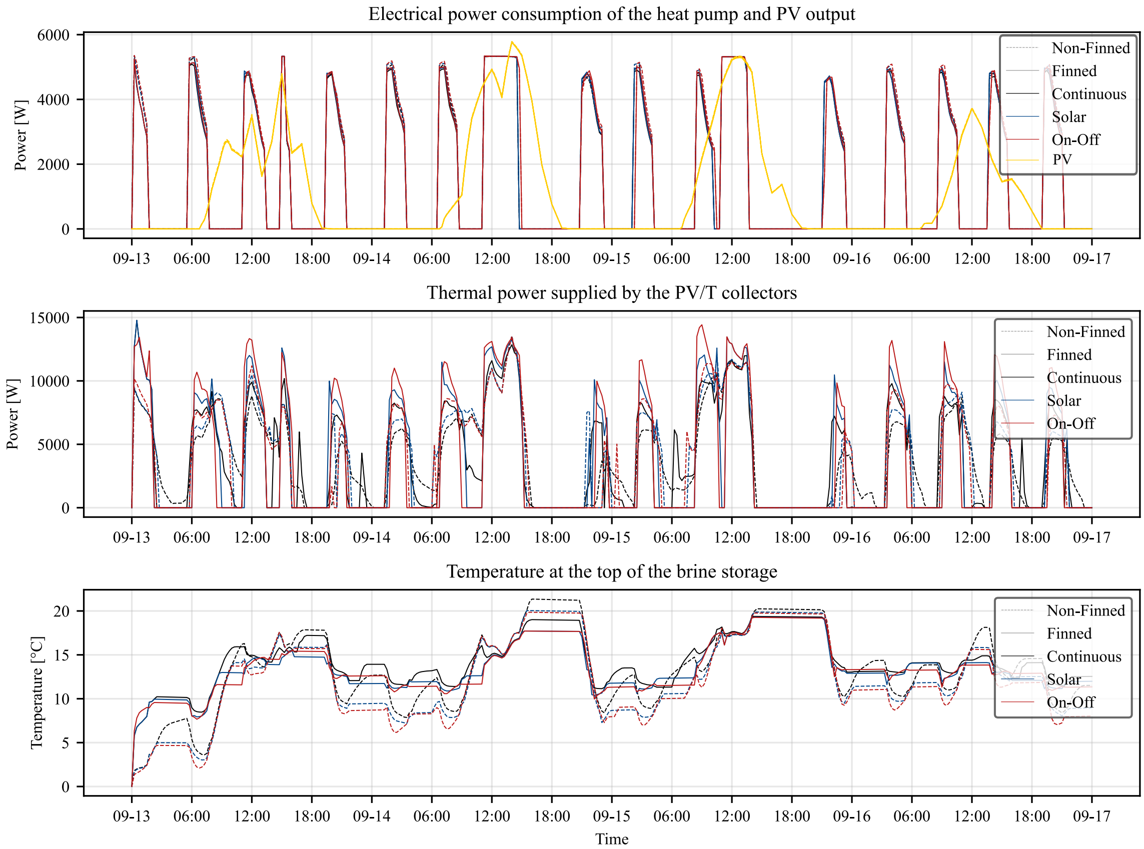

Fig. 4: Time-series of the control strategies and WISC types for a weather-independent load and a constant supply temperature of 60 °C.

applications with thermal load profiles that are largely independent of ambient temperature. The results for all three control strategies are presented in Figure 5. For the selected four-day period, a configuration with twenty finned and six non-finned WISCs per field results in a higher or comparable SPF_{Grid}, depending on the control strategy, than a field composed exclusively of finned WISCs. A preliminary collector-cost comparison showed that non-finned WISC types are, on average, 40 % cheaper than finned alternatives. For the test bench, this would reduce investment costs for the PV/T collectors by around 10 %. For applications with load profiles that enable greater utilization of the available solar energy, mixed configurations may offer additional cost reductions and improved operational efficiency. For the Continuous control strategy, configurations with a higher share of finned WISCs result in slightly lower SPF_{Grid} values, which highlights the potential of mixed WISC configurations in industrial PV/T heat pump systems.

Due to the base-load operation of the heat pump during the heating season, the brine pump operates mostly at full load. During this period, all three control strategies demonstrated similar behavior, resulting in only minor differences in the annual simulation results (Table 1). To evaluate the control strategies, the period in September (Figure 4), with a constant supply temperature of 60 °C, is analyzed separately. The corresponding results are given in brackets in Table 1. For both WISC types, the Continuous control strategy achieves the highest efficiency. This result confirms the findings presented by Ma et al. (2021). For the On–Off control strategy, the SPF_{Grid} of the finned WISC type is 6 % higher than that of the non-finned type, representing the largest observed difference. In contrast, the difference under the Continuous control strategy is only 3.7 %. A comparison of the control strategies within each WISC type shows an SPF_{Grid} difference of 3.5 % between the Continuous and On–Off control strategy for the finned type, whereas the difference for the non-finned type is 5.8 %. This indicates that the influence of the control strategy on system performance is stronger for the non-finned WISC type than for the finned type. This is attributed to the higher sensitivity of the thermal performance during periods of solar irradiation for the non-finned WISC type. In the annual simulation results, this effect is less pronounced but still evident.

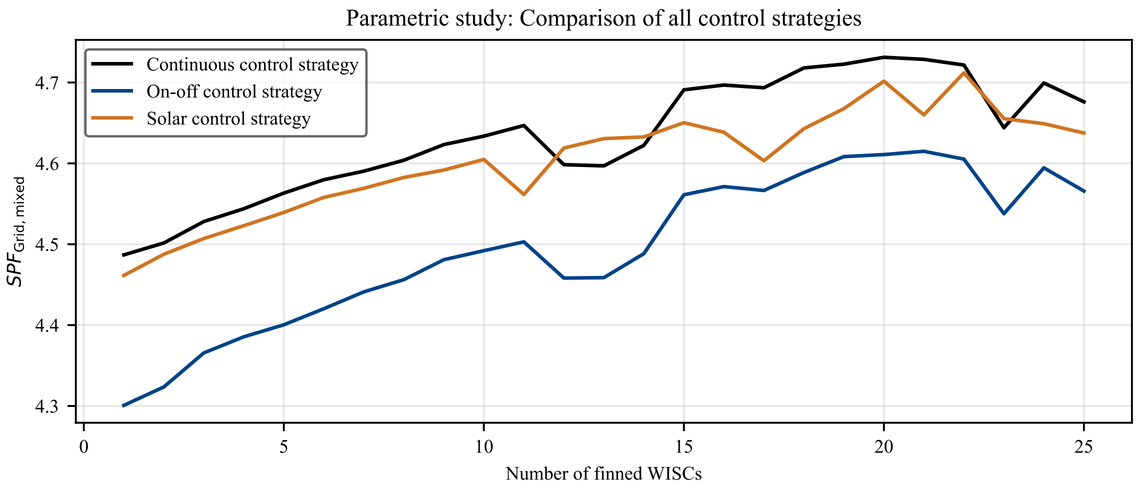

Fig. 5: Results of the parameter study for mixed WISC configurations during the four-day period in September. The total number of WISCs was fixed at twenty-six per heat pump. The number of non-finned WISCs $N_{\text{non-finned}}$ is given by: $N_{\text{non-finned}} = 26 - N_{\text{finned}}$

7. Conclusion

This study investigated the combined effects of collector type and source-side control strategy on the performance of a PV/T brine-to-water heat pump system for an industrial application. Finned, non-finned, and mixed WISC fields were evaluated using a Modelica-based simulation model. The key findings are:

- Finned WISCs achieved, on average, a 9 % higher SPF_{Grid} and the PV/T heat pump system supplied 4 % more thermal energy than non-finned WISCs. This advantage resulted primarily from higher ambient heat gains during periods of low or no solar irradiation.
- The Continuous control strategy achieved the highest SPF_{Grid} for both WISC types. However, the annual differences between the control strategies were small because the bivalent system configuration required the heat pumps and brine pump to operate predominantly at full load during the heating season.
- During the four-day period in September at a constant supply temperature of 60 °C, the Continuous control strategy increased the SPF_{Grid} by 3.5 % for the finned WISC and by 5.8 % for the non-finned WISC compared with the On-Off control strategy. Thus, the non-finned WISC was more sensitive to the source-side control strategy.
- For the four-day period in September, a mixed field comprising twenty finned and six non-finned WISCs achieved a higher or comparable SPF_{Grid} than an exclusively finned field, depending on the control strategy, while reducing the estimated collector investment cost by approximately 10 %.

Overall, the results show that collector selection and source-side control should not be considered independently when designing PV/T heat pump systems. Finned WISCs provide the highest annual efficiency for the investigated load profile, whereas mixed collector fields offer a promising compromise between system performance and investment cost. The Continuous control strategy is particularly beneficial for collector configurations with a high sensitivity to solar irradiation. Since the test bench is still under construction, the presented findings are based on simulations. Future work should validate the developed models and identified system configurations using experimental measurements from the PV/T heat pump test bench.

Nomenclature

Latin symbols

P_{el} Electrical power in W

E Electrical energy in kW h

$\dot{Q}_{th}$ Thermal power in W

Q Thermal energy in kW h

A_G Gross collector area in m^2

a_1 Heat loss coefficient in $W\,m^{-2}\,K^{-1}$

a_2 Temperature dependence of the heat loss coefficient in $W\,m^{-2}\,K^{-2}$

a_3 Wind speed dependence of the heat loss coefficient in $J\,m^{-3}\,K^{-1}$

a_4 Sky temperature dependence of the heat loss coefficient dimensionless

a_5 Effective thermal capacity per unit gross area in $J\,m^{-2}\,K^{-1}$

a_6 Wind speed dependence of the zero-loss efficiency in $s\,m^{-1}$

a_8 Fourth-order temperature loss coefficient in $W\,m^{-2}\,K^{-4}$

E_L Longwave irradiance in $W\,m^{-2}$

G_b Direct solar irradiance on the collector plane in $W\,m^{-2}$

G_d Diffuse solar irradiance on the collector plane in $W\,m^{-2}$

G_{beam} Beam irradiance in the transposition model in $W\,m^{-2}$

G_{diff} Diffuse irradiance in the transposition model in $W\,m^{-2}$

G_{refl} Ground-reflected irradiance on the collector plane in $W\,m^{-2}$

G_{tilt} Total irradiance on the tilted collector surface in $W\,m^{-2}$

K_b Incidence angle modifier for direct solar irradiance dimensionless

K_d Incidence angle modifier for diffuse solar irradiance dimensionless

R_b Geometric conversion factor for beam irradiance dimensionless

T_a Absolute ambient air temperature in K

t Time in s

x_{hp} Binary heat pump enable signal, where $x_{hp} \in \{0, 1\}$

u_{wind} Air speed parallel to the collector plane in $m\,s^{-1}$

Greek symbols

$\eta_{0,b}$ Peak collector efficiency based on direct solar irradiance dimensionless

σ Stefan–Boltzmann constant, $5.670 \times 10^{-8}\,W\,m^{-2}\,K^{-4}$

θ_L Longitudinal incidence angle in °

θ_T Transversal incidence angle in °

ϑ_a Ambient air temperature in °C

ϑ_m Mean heat transfer fluid temperature in °C

Abbreviations

COP Coefficient of performance

DWD German Meteorological Service

PV/T Photovoltaic-thermal

WISC Wind and infrared sensitive collector

References

Chhugani, B., Pärisch, P., Helmling, S., Giovannetti, F., 2023. Comparison of PVT - heat pump systems with reference systems for the energy supply of a single-family house. Solar Energy Advances 3, 100031. doi:10.1016/j.seja.2022.100031.

Del Amo, A., Martínez-Gracia, A., Bayod-Rújula, A.A., Cañada, M., 2019. Performance analysis and experimental validation of a solar-assisted heat pump fed by photovoltaic-thermal collectors. Energy 169, 1214–1223. doi:10.1016/j.energy.2018.12.117.

Duffie, J.A., Beckman, W.A., 2013. Solar Engineering of Thermal Processes. Wiley. doi:10.1002/9781118671603.

Epp, B., 2025. Marktübersicht offenbart Fortschritte und Defizite bei der PVT-Readiness [Market Overview Reveals Progress and Shortcomings in PVT Readiness]. HLH 76, 18–24. doi:10.37544/1436-5103-2025-11-12-18.

Fudholi, A., Sopian, K., 2018. R&D of Photovoltaic Thermal (PVT) Systems: an Overview. International Journal of Power Electronics and Drive Systems (IJPEDS) 9, 803. doi:10.11591/ijpeds.v9.i2.pp803-810.

Hengel, F., Heschl, C., Inschlag, F., Klanatsky, P., 2020. System efficiency of pvt collector-driven heat pumps. International Journal of Thermofluids 5-6, 100034. doi:10.1016/j.ijft.2020.100034.

International Organization for Standardization, 2025. ISO 9806:2025. URL: https://www.iso.org/standard/78801.html.

Jiang, D., Zhang, J., Lou, L., Lou, L., Zhu, K., Dai, J., 2025. Experimental investigation of the performance of a PVT heat pump soil cross-seasonal energy storage system across various operation modes. Energy 322, 135656. doi:10.1016/j.energy.2025.135656.

John, D., Kaltschmitt, M., 2022. Control of a PVT-Heat-Pump-System Based on Reinforcement Learning–Operating Cost Reduction through Flow Rate Variation. Energies 15, 2607. doi:10.3390/en15072607.

Kramer, K., 2024. PVT – nachhaltige Energietechnologie mit viel Effizienz [PVT – Sustainable Energy Technology with High Efficiency]. URL: https://websites.fraunhofer.de/ise-blog-innovation4e/2024/03/21/pvt-nachhaltige-energietechnologie-mit-viel-effizienz/. accessed 9 February 2026.

Kramer, K., Helmling, S., Fischer, S., 2025. Gemeinsamer Schlussbericht zum Projekt: Initiative zur Marktetablierung und Verbreitung von Anlagen zur thermisch-elektrischen Energieversorgung mittels PVT-Kollektoren und Wärmepumpen im Gebäudesektor [Joint Final Report on the Project: integraTE]. Schlussbericht 03EGB0023A/B/C.

Leibfried, U., Asenbeck, S., Fischer, S., Twerdy, C., 2020. Schlussbericht zum Förderprojekt: Hocheffiziente, auf intelligenter Verknüpfung von PVT- und Wärmepumpentechnik basierende Wärmeversorgung für Gebäudebestand und Neubau (Kurzbezeichnung SOLINK) [Final Report on the Grant Project: SOLINK]. Technical Report 33226/02.

Lämmle, M., 2018. THERMAL MANAGEMENT OF PVT COLLECTORS Development and modelling of highly efficient glazed, flat plate PVT collectors with low-emis s ivity coatings and overheating protection. Ph.D. thesis. Albert-Ludwigs-Universität Freiburg im Breisgau. Fraunhofer-Institut für Solare Energiesysteme (ISE).

Ma, J., Fung, A.S., Brands, M., Abul Moyeed, O.M., Mhanna, A., Juan, N., 2021. Effects of photovoltaic/thermal (PV/T) control strategies on the performance of liquid-based PV/T assisted heat pump for space heating. Renewable Energy 172, 753–764. doi:10.1016/j.renene.2021.02.030.

Maier, L., Jansen, D., Wüllhorst, F., Kremer, M., Kümpel, A., Blacha, T., Müller, D., 2026. AixLib: an open-source Modelica library for compound building energy systems from component to district level with automated quality management 17, 196–219. doi:10.1080/19401493.2023.2250521.

Mbuwir, B.V., Geysen, D., Kosmadakis, G., Pilou, M., Meramveliotakis, G., Toersche, H., 2024. Optimal control of a heat pump-based energy system for space heating and hot water provision in buildings: Results from a field test. Energy and Buildings 310, 114116. doi:10.1016/j.enbuild.2024.114116.

Modelica Association, 2026. Modelica. URL: https://modelica.org. accessed 8 July 2026.

Quaschning, V., 2023. Regenerative Energiesysteme: Technologie – Berechnung – Klimaschutz [Renewable Energy Systems: Technology – Calculations – Climate Protection]. Carl Hanser Verlag GmbH Co KG. doi:10.3139/9783446478398.

Ramos, C.A.F., Alcaso, A.N., Cardoso, A.J.M., 2019. Photovoltaic-thermal (PVT) technology: Review and case study. IOP Conference Series: Earth and Environmental Science 354, 012048. doi:10.1088/1755-1315/354/1/012048.

Solar Keymark, 2024. DIN CERTCO - Register-Nr. 011-7S2921 P. URL: https://www.dincertco.tuv.com/registrations/60138944. accessed 9 February 2026.

Solar Keymark, 2025. DIN CERTCO - Register-Nr. 011-7S3220 P. URL: https://www.dincertco.tuv.com/registrations/60174547. accessed 9 February 2026.

Wischhusen, S., 2005. Dynamische Simulation zur wirtschaftlichen Bewertung von komplexen Energiesystemen [Dynamic Simulation for the Economic Evaluation of Complex Energy Systems]. Ph.D. thesis. Technische Universität Hamburg-Harburg. Hamburg.

Wüllhorst, F., Reuter-Schniete, J., Maier, L., Hering, D., Müller, D., 2023. Heat Pump Systems with Photovoltaics: Influence of the Control Strategy on the Optimal Design, in: 36th International Conference on Efficiency, Cost, Optimization, Simulation and Environmental Impact of Energy Systems (ECOS 2023), ECOS 2023, Las Palmas De Gran Canaria, Spain. pp. 792–803. doi:10.52202/069564-0072.